Regional Flow Driven by Topographic Recharge

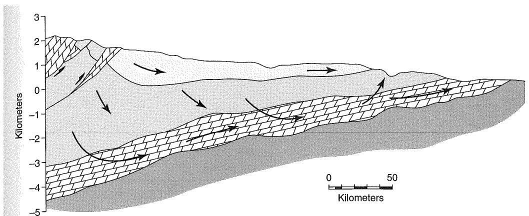

Figure 7.8 Conceptual model of topographically-driven flow in a foreland basin.
(From Garven and Freeze, 1984, p. 1091.)

Topographically Driven Flow

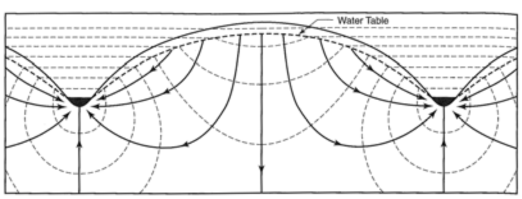

Figure 7.9 Topographically driven flow in a setting with alternating valleys and hills.
(From Toth, 1962; after Hubbert, 1940.)

Topographically Driven Flow

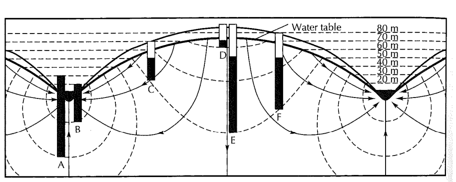

▲ FIGURE 7.2
Piezometers superimposed on Figure 7.1. The water level in the piezometer will rise to the elevation of the hydraulic head, which is represented by the equipotential line at the open end of the piezometer. Source: Modified from M. K. Hubbert, *Journal of Geology* 48, no. 8 (1940): 795–944. *Used with permission of the University of Chicago Press.*

Toth Model Boundary Conditions

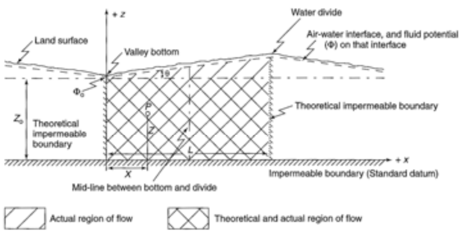

Figure 7.10 Toth model of topographically-driven flow in which alternating hills and valleys are approximated by trapezoids.
(From Toth, 1962, p. 4379.)

Toth Model Boundary Conditions

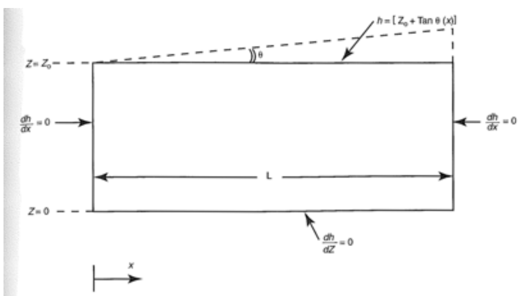

Figure 7.11 Boundary conditions and physical dimensions of Toth model of topographically driven flow.

Toth's Solution to Laplace's Eqn.

$$h = g\left(z_0 + \frac{\tan \alpha L}{2}\right) - \frac{4g \tan \alpha L}{\pi^2} \cdot \sum_{m=0}^{\infty} \frac{\cos[(2m+1)\pi x/L]\cosh[(2m+1)\pi z/L]}{(2m+1)^2\cosh[(2m+1)\pi z_0/L)]} \quad \textbf{(7.1)}$$

- h is the head (L)
- g is the gravitational constant (L/T^2)
- z_0 is the elevation of the water table at its lowest point above the bottom of the aquifer (L)
- z is the elevation of the water table above the bottom of the aquifer (L)
- $\tan \alpha$ is the slope of the water table
- L is the total length of the flow system (L)
- x is the horizontal distance from the place where the water table is at its lowest elevation (L)

Head Contours and Streamlines

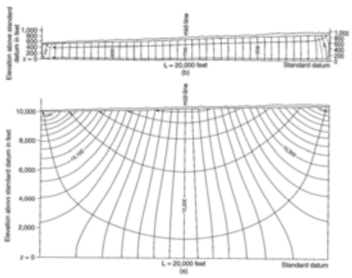

Figure 7.12 Head contours and streamlines in Toth model of topographically driven flow.
(From Toth, 1962, p. 4380.)

Sinusoidal Topography

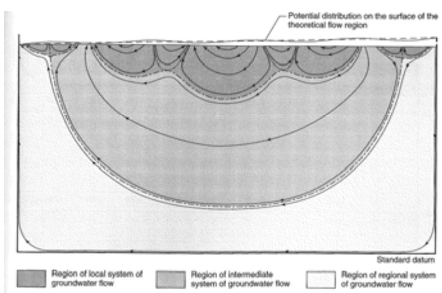

Figure 7.13 Head contours and streamlines in topographically-driven flow model with a sinusoidal topography.
(From Toth, 1963, p. 4807.)

Sinusoidal Topography

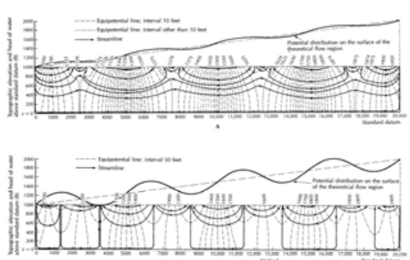

▲ FIGURE 7.5
The amplitude of the undulations of the water table controls the depth of local flow systems. For shallow basins, this can determine whether both local and regional flow systems will develop (Part A), or, with deeper undulations, only local flow systems will form (Part B). Source: J. A. Tóth, Journal of Geophysical Research 68 (1963): 4795–4811. Used with permission.

Effects of Water Table Configuration

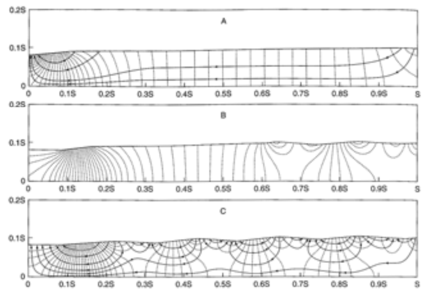

Figure 7.14 Effect of water table configuration and topography on regional groundwater flow through domains with homogeneous, isotropic hydraulic conductivity.
(From Freeze and Witherspoon, 1967, p. 625.)

Summary of Water Table Effects

In summary, Freeze and Witherspoon's modeling studies of topographically-driven groundwater flow showed that

1. Groundwater discharge tends to be concentrated in major valleys.
2. Recharge areas are invariably larger than discharge areas.
3. In areas with hummocky terrain, numerous sub-basins are superimposed on the regional flow system.

Stagnation Point

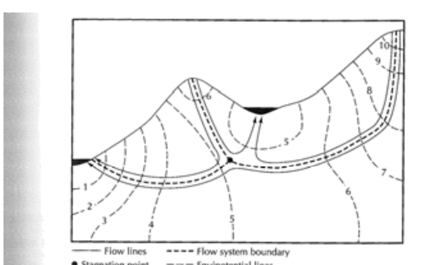

▲ FIGURE 7.6
The potential field and flow lines in the vicinity of a stagnation point, which will develop at the intersection of three flow systems.

Laplace's Equation (Variable K)

Laplace's equation in two dimensions,

$$\frac{d\left[-K_x \frac{dh}{dx}\right]}{dx} + \frac{d\left[-K_z \frac{dh}{dz}\right]}{dz} = 0 \qquad \textbf{(7.20)}$$

where K_x (m-s^{-1}) is the hydraulic conductivity in the horizontal dimension, and K_z (m-s^{-1}) is the hydraulic conductivity in the vertical dimension.

Aquifer Effects

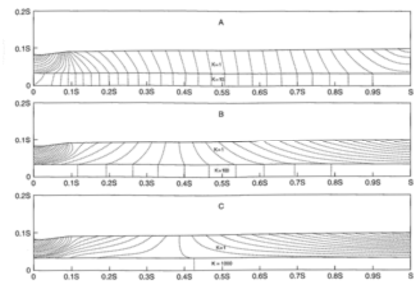

Aquifer Effects

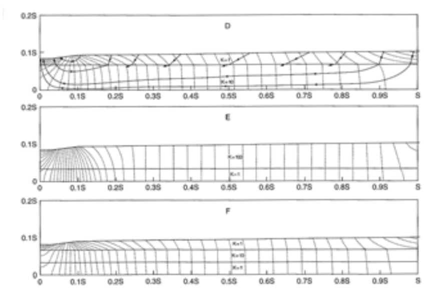

Figure 7.15 Regional groundwater flow through layered media with a simple water-table configuration, but contrasts in hydraulic conductivity between layers.
(From Freeze and Witherspoon, 1967, p. 627.)

Aquifer Effects

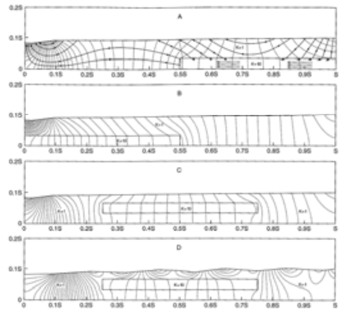

Figure 7.16 Regional groundwater flow through partial layers and lenses. The figure shows the effect on flow of a high permeability layer (K = 10) in a low-permeability (K = 1) medium.
(From Freeze and Witherspoon, 1967, p. 629.)

Summary of Aquifer Effects

4. Buried aquifers tend to concentrate flow toward the principal discharge area, limit the importance of sub-basins in producing small scale flow systems, and need not outcrop to produce artesian flow conditions.
5. Stratigraphic discontinuities can lead to distributions of recharge and discharge areas that are difficult to anticipate and that are largely independent of the water table configuration.

Density Driven Flow

$$\Delta h = \frac{(\bar{\rho}_1 z_1 - \bar{\rho}_2 z_2)}{\bar{\rho}} \qquad (7.22)$$

Differences in fluid density are caused by differences in salinity, temperature, and pressure. All of these factors are variable throughout the Earth's crust. Suppose that the difference between $\bar{\rho}_1$ and $\bar{\rho}_2$ is only 1%, such that $\bar{\rho}_1 = 1010$ kg-m^{-3}, and $\bar{\rho}_2 = 1000$ kg-m^{-3}. Then

$$\Delta h = \frac{10\ (\text{kg-m}^{-3}) \times 5000\ \text{m}}{1005\ (\text{kg-m}^{-3})} = 50\ (\text{m}) \qquad (7.23)$$

Density Driven Flow

The Darcy Velocity of the horizontal fluid flow between these two points is (from equation 2.55)

$$q = \frac{-k\bar{\rho}g}{\mu}\nabla h \qquad \textbf{(7.24)}$$

where k (m^2) is permeability and μ is fluid viscosity ($kg\text{-}m^{-1}\text{-}s^{-1}$). If we assume a typical crustal permeability of 10^{-15} m^2, fluid viscosity of 10^{-3} $kg\text{-}m^{-1}\text{-}s^{-1}$ (pure water at 150 °C, equation 4.23), then

$$q = \frac{10^{-15}\,\text{m}^2 \times 1005\ (\text{kg-m}^{-3}) \times 9.8\ (\text{m-s}^{-2})}{10^{-3}\ (\text{kg-m}^{-1}\text{-s}^{-1})} \times \frac{50}{10000}\,\frac{\text{m}}{\text{m}} \qquad \textbf{(7.25)}$$

$$q = 4.9 \times 10^{-11}\ (\text{m-s}^{-1}) \times 3.156 \times 10^{7}\ (\text{s-yr}^{-1}) = 0.0015\ (\text{m-yr}^{-1}) \qquad \textbf{(7.26)}$$

Density Driven Flow

Assuming a typical porosity of 10%, the linear velocity is ten times higher than the Darcy velocity (equation 2.19), thus

$$v = 0.015\ (\text{m-yr}^{-1}) \qquad \textbf{(7.27)}$$

This may not seem like much, but the time it takes to completely exchange the fluid between point 1 and point 2 is now

$$\text{time} = \frac{\text{distance}}{\text{velocity}} = \frac{10000\ (\text{m})}{0.015\ (\text{m-yr}^{-1})} = 6.7 \times 10^{5}\text{yr} \qquad \textbf{(7.28)}$$

In other words, there is a complete fluid exchange between points 1 and 2 every 670,000 years.

Rayleigh Analysis (Free Thermal Convection)

$$R_a = \frac{\alpha_T g \rho^2 C k y^2 \gamma}{\mu\lambda} \qquad \textbf{(7.29)}$$

where α_T (K^{-1} or $°C^{-1}$) is the coefficient of thermal expansion for a fluid, g ($m\text{-}s^{-2}$) is the acceleration due to gravity, ρ ($kg\text{-}m^{-3}$) is fluid density, C ($J\text{-}kg^{-1}\text{-}°K^{-1}$) is fluid specific heat capacity, k (m^2) is permeability, y (m) is height of the porous medium between boundaries, or cell height, γ ($K\text{-}m^{-1}$) is the thermal gradient, μ ($kg\text{-}m^{-1}\text{-}s^{-1}$) is the fluid dynamic viscosity, and λ ($W\text{-}m^{-1}K^{-1}$) is the thermal conductivity of the saturated porous medium.

Rayleigh Analysis (Free Thermal Convection)

The critical value of R_a at which convection begins in the porous medium described above is $4\Pi^2 \approx 40$ (Turcotte and Schubert, 1982, p. 405). If we apply a Rayleigh analysis to the continental crust, we may ask: for what value of permeability does convection begin? Rearranging equation 7.29,

$$k = \frac{40\mu\lambda}{\alpha g \rho^2 C y^2 \gamma} \quad \textbf{(7.30)}$$

Let $\alpha_T = 10^{-3}\ K^{-1}$, $g = 9.8\ m\text{-}s^{-2}$, $\rho = 1000\ kg\text{-}m^{-3}$, $C = 4200\ J\text{-}kg^{-1}\text{-}K^{-1}$, $y = 5000$ m, $\gamma = 0.025\ K\text{-}m^{-1}$, $\mu = 5 \times 10^{-4}\ kg\text{-}m^{-1}\text{-}s^{-1}$, and $\lambda = 2.5\ W\text{-}m^{-1}\text{-}K^{-1}$. We then find that

$$k = 1.9 \times 10^{-15}\ m^2 \quad \textbf{(7.31)}$$

Compilations of data by Brace (1984) and Clauser (1992) show that average permeabilities of crystalline rocks in the continental crust on the kilometer scale are of the order $10^{-15}\ m^2$; thus convection is apparently feasible over a representative range of thicknesses and thermal gradients.

Rayleigh Analysis (Free Thermal Convection)

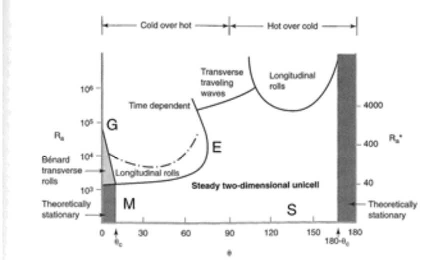

Figure 7.17 Convective flow regimes in a tilted porous medium as a function of tilt angle (Θ) and Rayleigh number (R_a).
(From Criss and Hofmeister, 1991, p. 200.)

Seismic Pumping

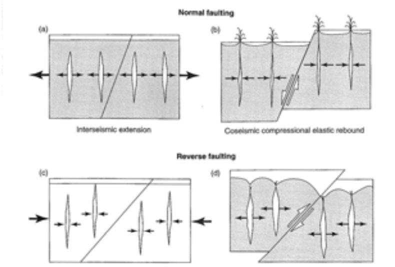

Figure 7.18 (a) In extensional terrains, porosity and fluid storage increase as strain builds up between earthquakes. (b) During and immediately following an earthquake on a normal fault, strain is released, porosity decreases, and fluids are expelled. (c) In compressional terrains, porosity and fluid storage decrease as strain builds up between earthquakes. (d) During and immediately following an earthquake on a reverse fault, strain is released, porosity increases, and fluids are absorbed.
(From Wood, 1994, p. 86.)

Seismic Pumping

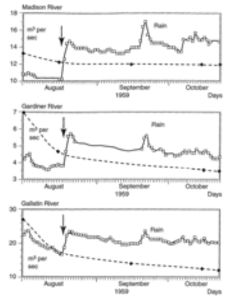

Figure 7.19 Stream discharge (thick line) as a function of time for three rivers in the vicinity of the 1959 Hebgen Lake earthquake in Montana. Stream flow increased immediately following the earthquake (arrow) even though there was no precipitation event. Dashed lines show average monthly discharge.
(From Wood, 1994, p. 87.)

Dilatational Jogs

Figure 7.20 Arrows illustrate flow into a dilatational jog immediately following fault movement.
(After Sibson, 1987, p. 702.)

Fault Valve Action

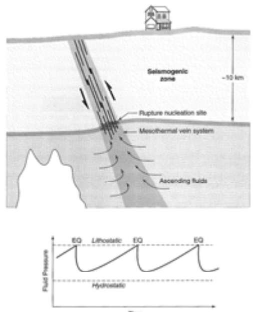

Figure 7.21 Schematic illustration (top) of fault-valve action wherein lithostatically-pressured fluids from the lower continental crust are released into the upper crust by rupturing related to a seismic event. Bottom figure shows cyclic nature of fluid pressure through time as repeated rupturing occurs.
(From Sibson, 1994, p. 80.)

Foreland Basins

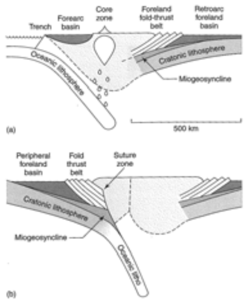

Figure 7.1 Plate tetonic settings in which foreland basins form.
(From Beaumont, 1981, p. 293.)

Intracratonic Basins

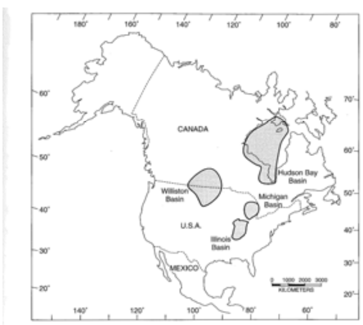

Figure 7.2 Location of major intracratonic basins in North America.
(From Klein, 1991, p. 4.)

Pull-Apart Basin

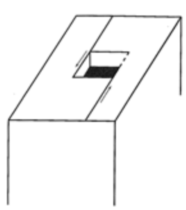

Figure 7.3 Conceptual illustration of how a strike-slip or pull-apart basin forms at an offset in a strike-slip fault.

Sedimentation Rates

Table 7.1 Average Sedimentation Rates.

Geologic Setting	Sedimentation Rate ($m \cdot Ma^{-1}$)
intracratonic basins	~10
rift basins	~50–100
foreland basins	~100
strike-slip/forearc	~100–1,000
river deltas	~1,000–10,000

Compaction Driven Flow

$$q = \frac{0.5RA}{A} = 0.5R \qquad (7.3)$$

In other words, the average Darcy velocity of fluid flow due to sediment compaction is proportional to the sedimentation rate and is of the same order of magnitude. Sedimentation rate varies with the geologic setting (Table 7.1).

Tectonic Subsidence

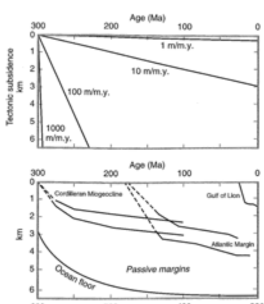

Tectonic Subsidence

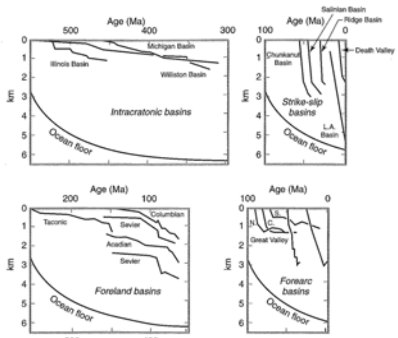

Subsidence/Uplift of Basins

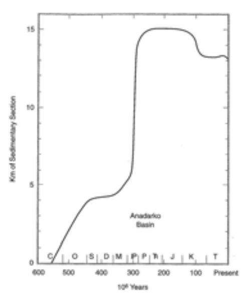

Figure 7.5 Sediment thickness/subsidence of the Anadarko Basin as a function of time. (From Gilbert, 1992, p. 205.)

Changes in T, P, n with burial

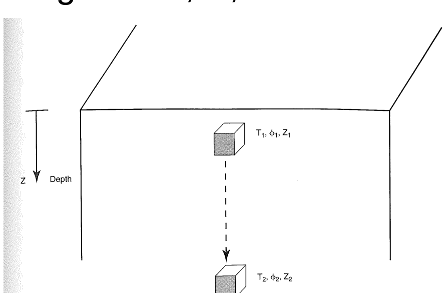

Figure 7.6 A control volume of rock or sediment in a sedimentary basin evolves from a depth Z_1, temperature T_1, and porosity ϕ_1, to a depth Z_2, etc.

Compaction vs. Aquathermal Pressure

$$\frac{d\rho}{\rho} = BdP - \alpha_T dT \qquad \textbf{(7.4)}$$

where ρ ($kg\text{-}m^{-3}$) is fluid density, B ($m\text{-}s^2\text{-}kg^{-1}$) is the isothermal fluid compressibility (as defined in equation 3.24), P ($kg\text{-}m^{-1}\text{-}s^{-2}$) is fluid pressure, α_T (K^{-1} or $°C^{-1}$) is the coefficient of thermal expansion of the fluid, and T (K or °C) is temperature.

Compaction vs. Aquathermal Pressure

$$\frac{dV}{V} = -BdP + \alpha_T dT \qquad \textbf{(7.9)}$$

Now, to calculate the increase in fluid pressure associated with heating the pore fluid, suppose the pore fluid is heated but cannot expand because the pore space is constant. Constant fluid volume implies that $dV/V = 0$, thus

$$BdP = \alpha_T dT \qquad \textbf{(7.10)}$$

or

$$dP = \alpha_T \frac{dT}{B} \qquad \textbf{(7.11)}$$

Compaction vs. Aquathermal Pressure

Alternatively, to calculate the increase in fluid pressure that occurs from pore collapse alone, suppose that temperature is held constant, but that the pore space changes. Then $dT = 0$ in equation 7.9, and

$$\frac{dV}{V} = -BdP \qquad \textbf{(7.12)}$$

or

$$dP = \frac{-\frac{dV}{V}}{B} \qquad \textbf{(7.13)}$$

Compaction vs. Aquathermal Pressure

$$\text{ratio} = \frac{\alpha_T \Delta T}{\frac{\Delta V}{V}} \qquad \textbf{(7.15)}$$

To evaluate the magnitude of this ratio, consider an average sedimentation rate of 50 m-Ma^{-1} for 1 Ma. Assume that the change of porosity of depth may be described by an exponential model, $\phi = \phi_0 e^{-z/b}$, and take $\phi_0 = 0.25$ and $b = 3000$ m. Let the coefficient of fluid thermal expansion (α_T) be 5×10^{-4} K^{-1}. Choose $z_1 = 1000$ m depth, $z_2 = 1050$ m depth, and assume an average geothermal gradient of 25°C-km^{-1}. Then $\phi_1 = 0.17913$, $\phi_2 = 0.17617$, and $\Delta\phi = \phi_1 - \phi_2 = 0.00296$. Define the average porosity as $\bar{\phi} = (\phi_1 + \phi_2)/2 = 0.17765$. We can then approximate $\Delta V/V$ by $\Delta\phi/\bar{\phi} = 0.00296/0.17765 = 0.01667$. The change in temperature from z_1 to z_2 is 1.25 °C. Thus

$$\text{ratio} = \frac{(5 \times 10^{-4})(1.25)}{0.01667} = \frac{1}{27} \qquad \textbf{(7.16)}$$

Compaction Driven Flow

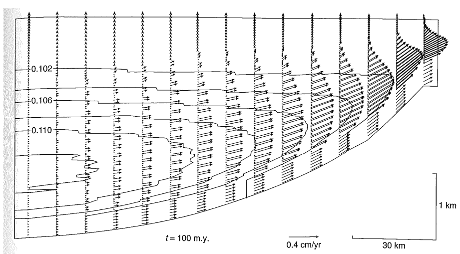

Figure 7.7 Linear flow velocities as calculated by a two-dimensional model of fluid flow in an intracratonic basin driven by sediment compaction. Heavy lines are fluid equipotentials in Mpa. Vertical exaggeration is 25:1.
(From Bethke, 1988, p. 3502.)

Compaction Driven Flow

1. Fluids expelled from shallow sediments move upwards, while deeper fluids move laterally to basin edges (Figure 7.7).
2. Very small excess pressures (exceeding hydrostatic) develop.

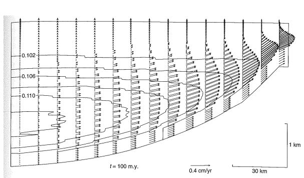

Figure 7.7 Linear flow velocities as calculated by a two-dimensional model of fluid flow in an intracratonic basin driven by sediment compaction. Heavy lines are fluid equipotentials in Mpa. Vertical exaggeration is 25:1.
(From Bethke, 1988, p. 3502.)

Compaction Driven Flow

3. Fluid velocity scales with sedimentation rate. Maximum linear velocity is about 0.5 cm-yr^{-1}; average linear fluid velocity is about 0.2 cm-yr^{-1}.
4. Compaction-driven fluid flow in intracratonic basins is not an efficient mechanism for heat and mass transport
5. Interlayered sands and shales lead to a very high basin-scale anisotropy, k_x/k_z ~ 1000.

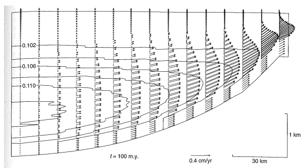

Figure 7.7 Linear flow velocities as calculated by a two-dimensional model of fluid flow in an intracratonic basin driven by sediment compaction. Heavy lines are fluid equipotentials in Mpa. Vertical exaggeration is 25:1. (From Bethke, 1988, p. 3502.)

Compaction Driven Flow

6. Expelled pore fluids tend to move vertically out of compacting shales (aquitards) into neighboring sandstone aquifers and then travel horizontally to basin edges (Figure 7.7).
7. Some pore fluids move downwards (inspect the isopotentials in Figure 7.7). Near the center of the basin, the path of least resistance may be for pore fluids to move downwards to a basal aquifer and then laterally to the basin edge.
8. In stark contrast to topographically driven flow, flow velocities are not dependent upon permeability so long as the actual compaction process itself is not inhibited or retarded.

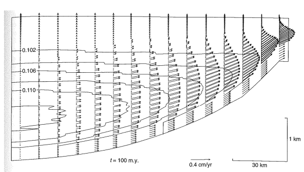

Figure 7.7 Linear flow velocities as calculated by a two-dimensional model of fluid flow in an intracratonic basin driven by sediment compaction. Heavy lines are fluid equipotentials in Mpa. Vertical exaggeration is 25:1. (From Bethke, 1988, p. 3502.)

Compaction Driven Flow

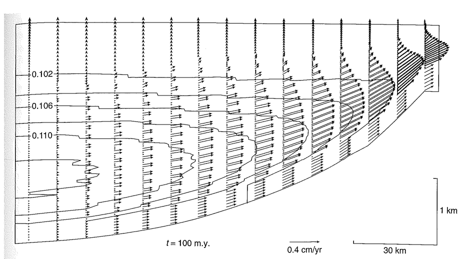

Figure 7.7 Linear flow velocities as calculated by a two-dimensional model of fluid flow in an intracratonic basin driven by sediment compaction. Heavy lines are fluid equipotentials in Mpa. Vertical exaggeration is 25:1. (From Bethke, 1988, p. 3502.)

Natural Springs

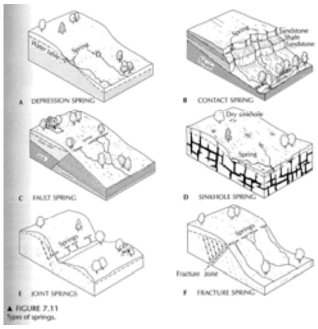

▲ FIGURE 7.11
Types of springs.

Photos of Springs